2

Realization of 12-Element MIMO Antenna for 5G Smartphones

*A compact two-element MIMO antenna with improved impedance matching and isolation is presented for 5G sub-6 GHz applications, in this chapter. The two identical tapered microstrip line fed modified rhombus-shaped radiating elements are placed in the same orientation on a rectangular substrate with a shared ground plane. A remodeled T-shaped ground stub is placed between a pair of radiating elements to achieve improved impedance bandwidth and isolation. A split U-shaped stub connected to centre of each radiating element to achieve the desired resonant frequency of 3.6 GHz. The proposed antenna has a -10 dB operating band of 3.34-3.87 GHz (530 MHz) with more than 20 dB isolation between a pair of elements. The measured performances of a prototype are found in good agreement with simulated performances. Further, the simulation study is carried out to see the effect of housing and extended ground plane on two-element MIMO antenna for practical application, found satishfactory results suitable for extending to a higher-order MIMO antenna. As a result, an idea of realization of 12-element MIMO antenna is also studied using two-element MIMO antenna, exhibits characteristics appropriate for 5G smartphones **

*Parts of this chapter have been published: Arun Kumar Saurabh and Manoj Kumar Meshram, "Compact sub-6 GHz 5G-multiple-input-multiple-output antenna system with enhanced isolation," *International Journal of RF and Microwave Computer-Aided Engineering,* vol. 30, no. 8, pp. 1-11, 2020.

2.1 Introduction

The 5G (Fifth-Generation) technology has been attracted more attention of the researchers in recent year. 5G wireless communication system is looking forward as a new generation system, which has ensured data rates in Gb/s, terminal latency rates in millisecond, and system capacity thousand times that of the long-term evolution (LTE) 4G wireless system [92]. The 5G-MIMO antenna system is a promising technology in realizing the 5G New Radio (NR) standard, which can increase the system capacity by deploying a larger number of antenna elements. It ensures distinct features likes extremely high data rate, a highly large channel capacity, extremely low latency, and high quality of service within restricted amount of power in the highly scattered environment of modern wireless communication systems involving 5G technology after 4G [93]. 5G wireless communication systems will support spectrum band of sub-6 GHz (spectrum bellow 6 GHz) and millimeter-wave (spectrum above 24 GHz). Recently, the wireless communication industries in many countries are mainly focused on the frequency band of sub-6 GHz (3.4-3.8 GHz) [94] and millimeter-wave (24.25-27.5 GHz) [95]. The antenna size is the one of the main constraint for researchers because the area available for the placement of multiple antenna elements in portable/compact devices is restricted. It can be mitigated by designing compact closely spaced antenna elements. Due to which mutual coupling between a pair of antenna elements increased, hence performances of MIMO system degrades [96], [97]. It is more challenging to achieve high isolation between the compact and closely positioned antenna elements having shared ground plane in the MIMO system.

Various methods have been published in the literature to improve the isolation between a pair of antenna elements of the MIMO systems. A vertical slit created on the T-shaped ground stub [98], inverted L-shaped [62], and F-shaped ground stub [60] were

used in the two-element UWB-MIMO system to enhance the isolation. A narrow rectangular stub was placed between T-shaped stubs connected to feed lines of the two-element MIMO system for low mutual coupling in [64]. In [54], a decoupling parasitic T-shaped strip was placed between two-element MIMO system for high isolation. A radial stub loaded resonator (RSLR) based T-shaped ground stub was utilized to enhance the isolation [99]. A tree-like structure-based ground stub was used for wideband isolation between antenna elements [44]. A wideband neutralization line [56], coupled resonator decoupling network (CRDN) [100] were also used to reduce the coupling between the antenna elements. The metasurface superstrate was used to reduce the coupling between closely spaced antenna element [101], [102], [103]. The coupling between closely spaced two-element antennas was reduced by using different variant of metamaterial superstrate such as combination of dual split–ring unit cell and neutralization line [104], flower shaped [105], 3-D metamaterial [106], multi-layered electromagnetic band gap (ML-EBG) [107]. A shorting pin was used between two symmetrically placed radiator for low mutual coupling. Further, coupling was reduced with the help of four choke groves on the ground in the 8-element 5G-MIMO antenna below Sub-6 GHz in [108]. The tapered microstrip line, and meandered line technique were reported for better impedance matching of MIMO system in [109], [110]. However, the above-discussed two-element MIMO antennas were mostly designed for UWB (Ultrawideband) and WLAN (Wireless Local Area Networks) applications with larger in size and moderate isolation.

In this chapter, a closely spaced compact two-element sub-6 GHz 5G-MIMO antenna system with shared ground plane is proposed. The proposed antenna contains two modified rhombus-shaped radiators fed through tapered microstrip line, partial rectangular ground plane. A remodeled T-shaped ground stub is placed between radiating elements to achieve simultaneous improvement in impedance matching and isolation.

Further, split U-shaped stub is placed at the centre of each radiator of the MIMO antenna for simultaneous improvement in impedance matching with decrease in the resonant frequency. Additionally, simulation study is carried out using the proposed 2-element MIMO for the realization of 12-element MIMO antenna configuration for 5G application. The details of design and characterization are given in following sections.

2.2 Details of 2-Element MIMO Antenna

Fig. 2.1 illustrates a final geometry of two-element MIMO antenna having total projected volume of $20\times35\times0.8$ mm^3 or about $0.24\lambda_0\times0.42\lambda_0\times0.0096\lambda_0$, where λ_0 is the resonant wavelength at 3.6 GHz, which is designed on FR4-epoxy substrate (ε_r = 4.4, $tan\ \delta$ = 0.02, h = 0.8 mm). To make proposed MIMO configuration compact and closely spaced, the elements are separated by $0.108\lambda_0$. The simulation study is carried out using ANSYS HFSS. To evolve the configuration of the proposed antenna, four different cases are considered which are termed as Case_1 to Case_4, respectively in the paper as shown in Fig 2. In the beginning, we have selected simple planar rectangular monopole radiator. The modified rhombus-shaped monopole radiator is achieved with a combination of the rectangle, half-circle, and trapezium having a rectangular ground plane, fed through tapered microstrip line for better impedance matching. The dimensions of radiating elements, ground, and gap between radiating element and ground plane are optimized for proper impedance matching, isolation, and the targeted resonant frequency of 3.6 GHz.

2.2.1 Design Evolution and Corresponding *S*-parameters

The design evolution of the proposed antenna and corresponding *S*-parameters are depicted in Fig. 2.2 and 2.3 respectively. The two identical rectangular radiating elements having same orientation and a common rectangular ground plane ($L_{g1}\times W$) are arranged at top and bottom of substrate cross-section ($L\times W$) respectively, which is fed through 50Ω

tapered microstrip line which resulted in poor *S*-parameters, shown in Fig. 2.2(a) considered as Case_1. In Case_2, rectangular radiating elements are modified and a T-shaped ground stub is placed between a pair of radiating elements, which acts as a reflector and decoupling structure. It provides better *S*-parameters performances in terms of impedance matching and isolation between a pair of antenna elements, as shown in Fig. 2.2(b). In Case_3, modified rhombus-shaped monopole elements with a remodeled T-shaped ground stub are placed by further alteration in Case_2, resulted in the decrease of resonant frequency and operating band with increased isolation, as illustrated in Fig. 2.2(c).

The fundamental lower resonant frequency of the configured single antenna element of the MIMO antenna considered in Case_3 is approimated using Eq. (2.1).

$$f_r = \frac{144}{l_g + l_{rp} + g_{grp} + \frac{A_g}{2\pi l_g \sqrt{\varepsilon_{reff}}} + \frac{A_{rp}}{2\pi l_{rp} \sqrt{\varepsilon_{reff}}}} \quad \text{GHz} \tag{2.1}$$

where,

$l_g = L$,

$l_{rp} = L_2/2 + L_6 + (L_1 - L_8 - L_7/2 - L_2/2 - L_{10} - L_{11} - L_{12})$,

$g_{grp} = L_9 - L_{g1}$,

$A_g = [L_{g1}W - (L - L_{g1} - L_{g2})W_{g1} + (L_{g2}W_{g2} - \pi L_{g2}^2/2)]$,

$A_{rp} = [L_6W_7 + 3\pi L_2^2/2 - 2(L_4W_6 + L_4W_6 + L_5W_5) - 2(L_{g11}W_9 + L_{g12}W_9 + L_{g12}W_{10}) + \{(L_1 - L_8 - L_7/2 - L_2/2 - L_{10} - L_{11} - L_{12})(W_2 + W_{f1})/2\} + L_9(W_2 + W_{f1})/2]$.

The obtained first resonating frequency (f_r) for Case_3 is 4.474 GHz, which is almost close to the simulated value of 4.5 GHz.

Further, to achieve the targeted resonant frequency at 3.6 GHz of 5G NR (New Radio) application with simultaneous improvement in impedance matching and isolation, split U-shaped stub ($\lambda_g/2$ length of the stubs) is attached at the centre of radiating elements of the proposed antenna which provides satisfactory MIMO performances for 5G applications, depicted in Fig. 2.2(d) considered as Case_4. Fig. 2.3 shows the simulated *S*-parameters performances corresponding the four cases considered as Case_1

to Case_4. The radiating elements of the MIMO antenna are identical due to which reflection and coupling *S*-parameters are identical.

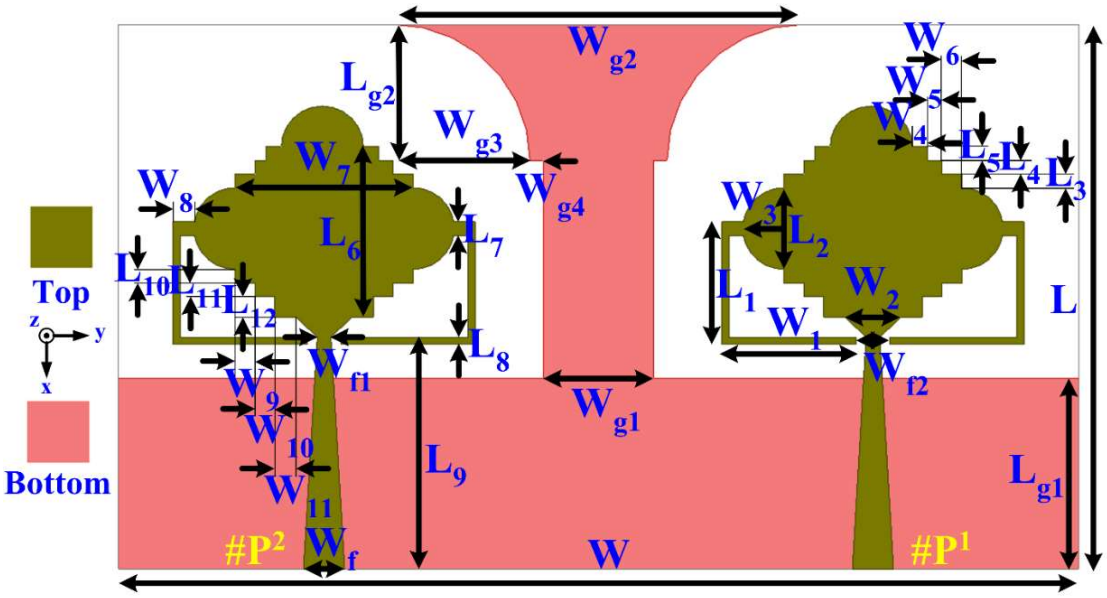

Fig. 2.1: Final configuration of the MIMO antenna with optimized parameters. Dimensions (*in mm*): L=20, W=35, L_{g1}=7, L_{g2}=5, W_{g1}=4, W_{g2}=15, W_{g3}=5, W_{g4}=0.5, W_f=1.5, W_{f1}=0.5, W_{f2}=1.25, L_1=4.5, L_2=3, L_3, L_4, L_5=0.5, L_6=6.25, L_7=0.5, L_8=0.25, L_9=8.5, L_{10}, L_{11}=0.5, L_{12}=0.75, W_1=4.875, W_2=2.05, W_3=1.5, W_4=0.5625, W_5=0.5, W_6=0.75, W_7=6.5, W_8=0.771, W_9=0.75, W_{10}=0.7, W_{11}=0.775.

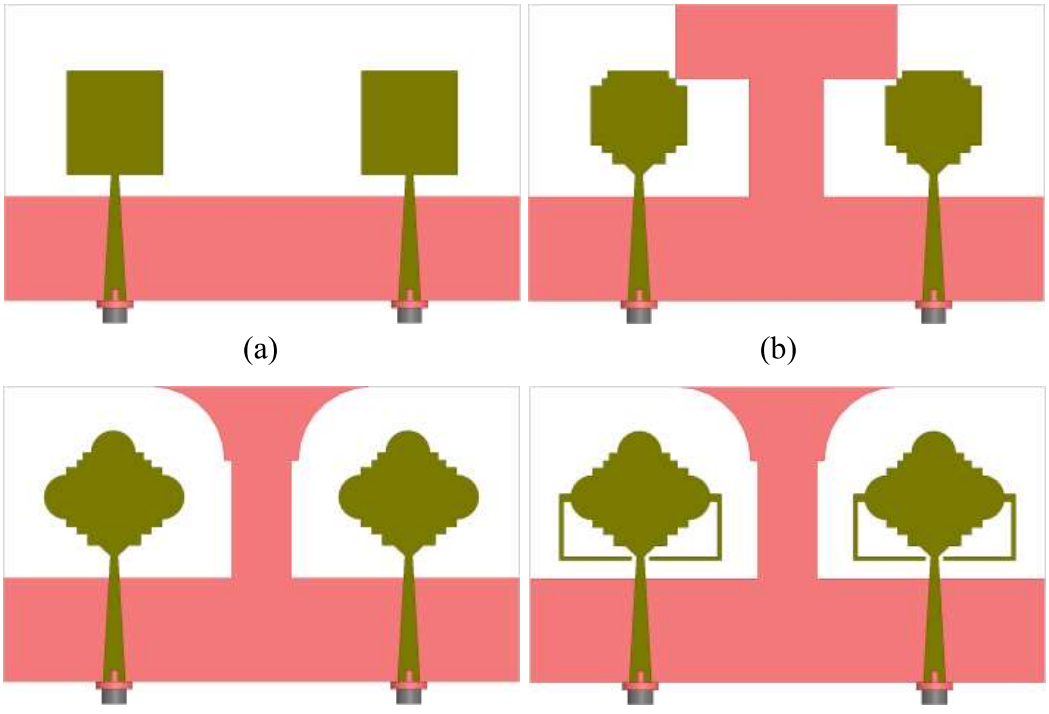

Fig. 2.2: Design evolution of MIMO antenna (a) Case_1, (b) Case_2, (c) Case_3, and (d) Case_4.

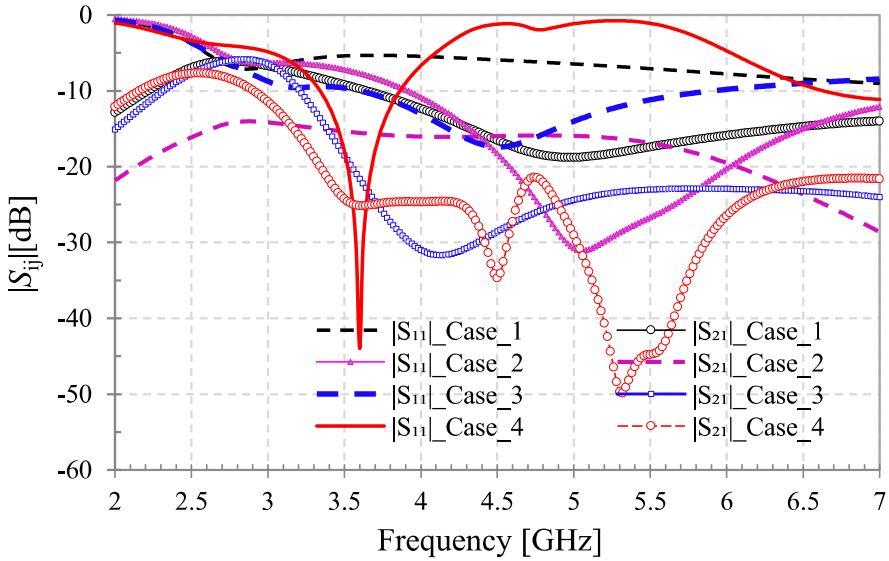

Fig. 2.3: *S*-parameters characteristics of the MIMO antenna for different cases.

2.2.2 Input Impedance

The variation of input impedance (Z_{11}) is depicted in Fig. 2.4. It is clearly noticed that the resonant frequency occurred at 3.6 GHz. The real and imaginary value of input impedance are 50.5Ω and 0Ω, respectively at 3.6 GHz. It is quite clear from Fig. 4 that near the resonant frequency, the proposed antenna behaves like series resonance circuit consisting of resistance (R), inductance (L), and capacitance (C) connected in series. This series circuit provides zero effective reactance and minimum effective resistance at the resonant frequency. At other frequencies near resonant frequency, the proposed antenna provides effective capacitive and inductive reactance on lower and higher frequency sides respectively. As the frequency reduces further below the resonant frequency (outside the proposed antenna passband) antenna behavior changes from series resonant circuit to parallel resonant circuit gives rise to resistance peak at resonance and conversion of effective capacitive reactance to inductive reactance passing through zero. On the other hand on higher side of resonant frequency as frequency increases further (outside the proposed antenna passband) antenna behavior changes from series resonant circuit to parallel resonant circuit again gives rise to resistance peak at resonance and conversion of effective inductive reactance to capacitive reactance passing through zero.

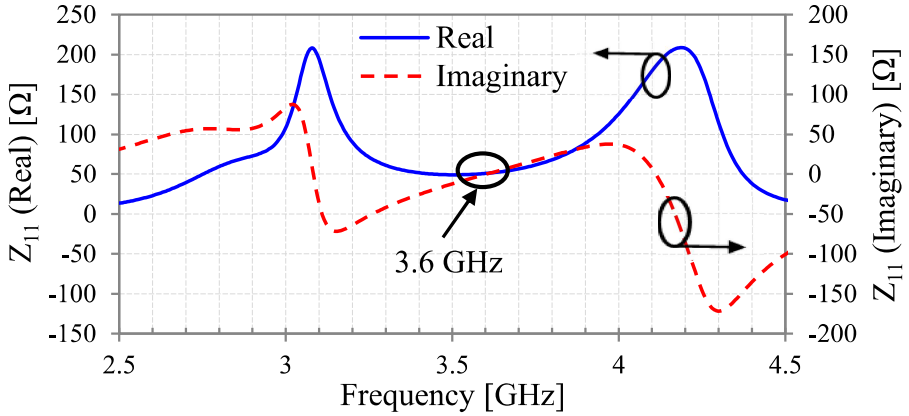

Fig. 2.4: Input impedance of MIMO antenna considered in Case_4.

2.2.3 Current Distribution Plot

To understand the simultaneous improved in impedance matching and isolation, current distribution is plotted on the surface of the ground plane and radiating elements at 3.6 GHz, without and with the radiating stub in Fig. 2.5, when element-1 (#P^1) is kept excited and element-2 (#P^2) is matched terminated. From Fig. 2.5(a), it is observed that the orientation of the current is concentrated to feed line and the boundaries of the remodeled T-shaped ground stub. Some amount of current is flowing in radiating element-2 through ground stub; therefore moderate matching occurred. Similarly, from Fig. 2.5(b), it is observed that the orientation of the current is highly concentrated to feed line and right boundaries of the radiating element having right radiating stub and some part of the current are flowing in the boundaries of the ground stub and radiating element-2. Therefore, high impedance matching and isolation between a pair of element is resulted, due to the strong current density on the surface of the presented MIMO antenna. Fig. 2.5(c) shows the vector current distribution, when element-1 is excited and element-2 is kept matched terminated. It is clearly observed that the strong current is distributed from element-1 however; the highly concentrated vector current on each antenna is orthogonal to each other and accommodates one-half wavelength at corresponding to the resonating frequency. Hence the arriving current at the element-2 is very weak due to which low mutual coupling is obtained.

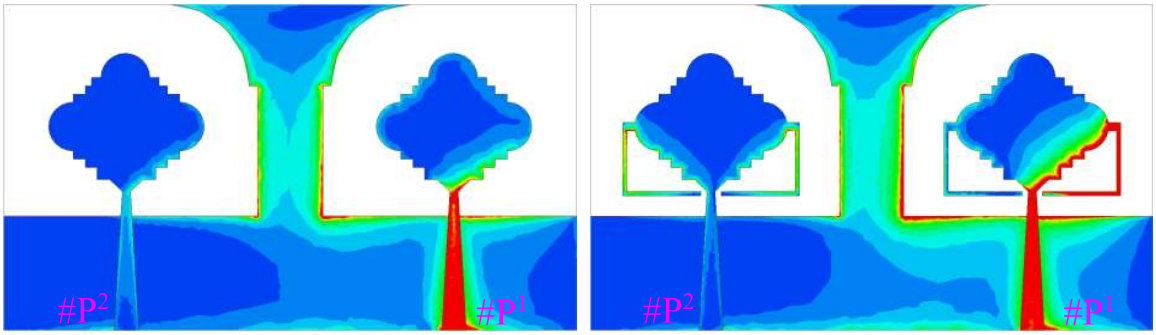

(a) (b)

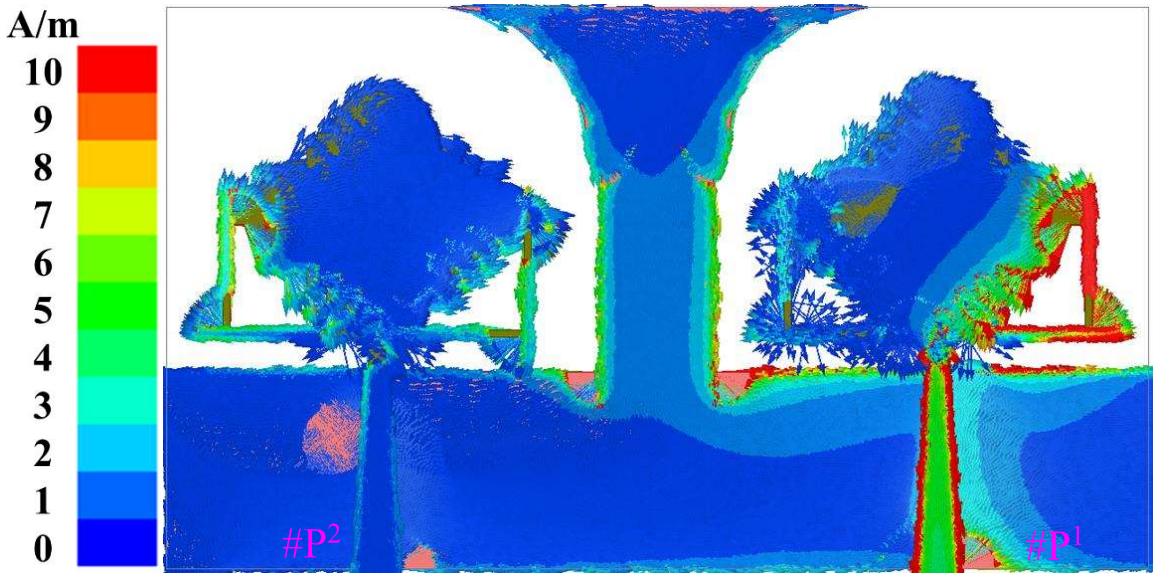

(c)

Fig. 2.5: Surface current distribution of the MIMO antenna at 3.6 GHz (a) without radiating stub, (b) with radiating stub, and (c) vector current plot.

2.2.4 Ground and Radiator Stubs Length

The ground stub length ($\lambda_g/2$) is calculated using Eq. (2.2) at the resonant frequency of 3.6 GHz. Similarly, the length of the U-shaped stub is also calculated which is almost close to $\lambda_g/2$.

$$L_{3.6} = \left[\frac{W_{g1}}{2} + \frac{W_{g2}}{2} + \frac{2\pi W_{g3}}{4} + W_{g4} + (L - L_{g1} - L_{g2})\right] \cong 0.5\lambda_g \tag{2.2}$$

$$\lambda_g = \frac{c}{f_r\sqrt{\varepsilon_{eff}}} \tag{2.3}$$

$$\varepsilon_{eff} \cong \frac{\varepsilon_r + 1}{2} \tag{2.4}$$

where λ_g is the guided wavelength, c is the speed of light, f_r is the resonating frequency, ε_r is the relative permittivity, and ε_{eff} is effective relative permittivity of the substrate.

2.3 Results and Discussion

2.3.1 *S*-parameter Results

In Fig. 2.6(a)-(b), the top and bottom view of a prototype are illustrated, respectively, and corresponding *S*-parameters (simulated and measured) results are depicted in Fig. 2.6(c). The presented MIMO antenna has a simulated -10 dB impedance bandwidth of 530 MHz over a frequency band of 3.34-3.87 GHz with impedance matching of -44 dB and isolation value more than 20 dB is obtained between antenna pairs. The measured *S*-parameters outcomes of the prototype are found in similitude with simulated. The discrepancy occurred dominantly due to manufacturing and soldering tolerances. The measured -10 dB frequency band of 3.34-3.79 GHz with a minimum isolation value of -15 dB is observed which satisfy the acceptable limit for practical 5G wireless applications.

2.3.2 Radiation Pattern

In Fig. 2.7, the simulated and measured 2-D radiation patterns of the MIMO antenna are illustrated in two principal planes (xz and yz) at 3.6 GHz when element-1 (#P^1) is excited and element-2 (#P^2) is kept matched terminated. The omnidirectional pattern with appropriate co-to-cross polar isolation is observed. The simulated and measured radiation patterns are found in similitude.

Fig. 2.8 shows the 3-D radiation patterns of the MIMO antenna at 3.6 GHz when element-1 (#P^1) is excited and element-2 (#P^2) is kept matched terminated. The omnidirectional pattern is observed at 3.6 GHz with a 2.34 dBi peak gain value which is also corroborated in Fig. 2.7.

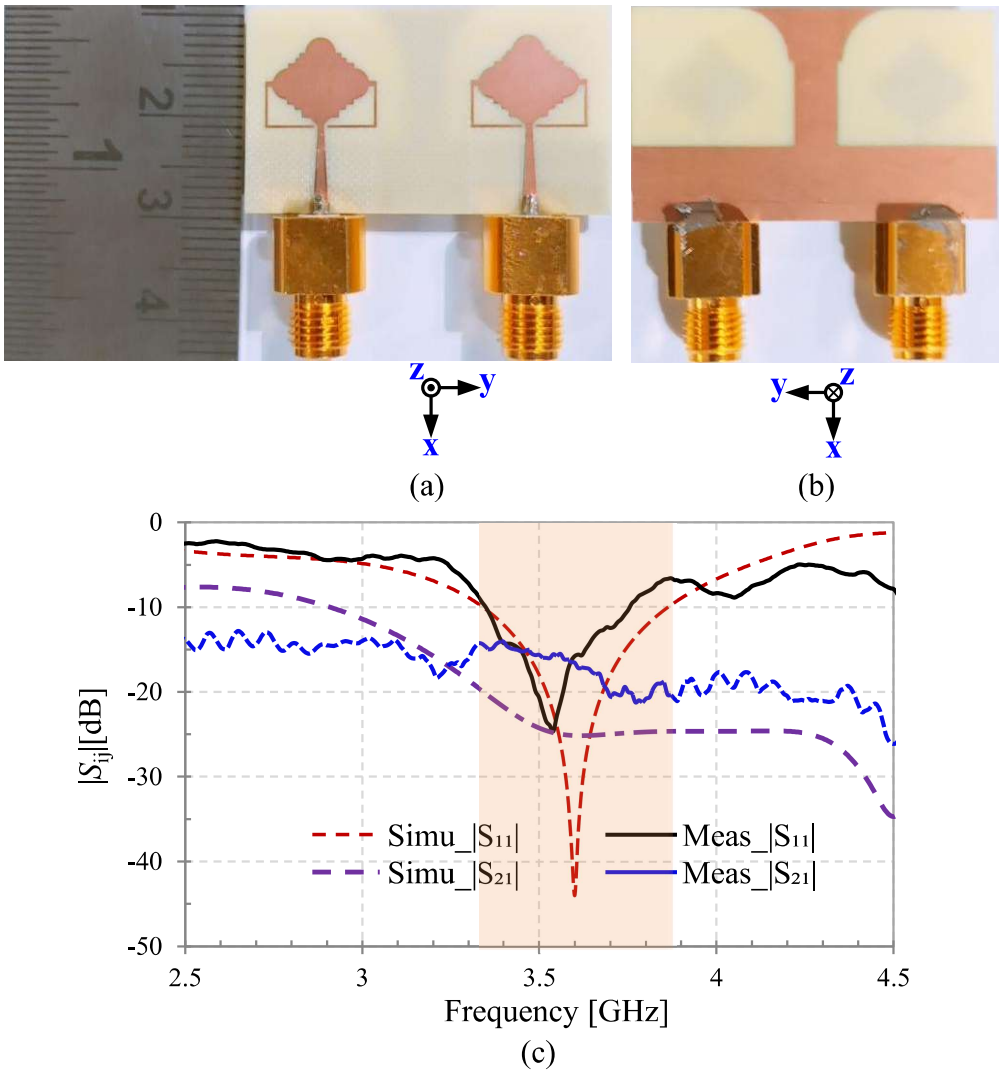

Fig. 2.6: View of the prototype (a) top, (b) bottom, and (c) corresponding simulated and measured *S*-parameters characteristics.
Abbreviation: Simu = simulated, Meas = measured.

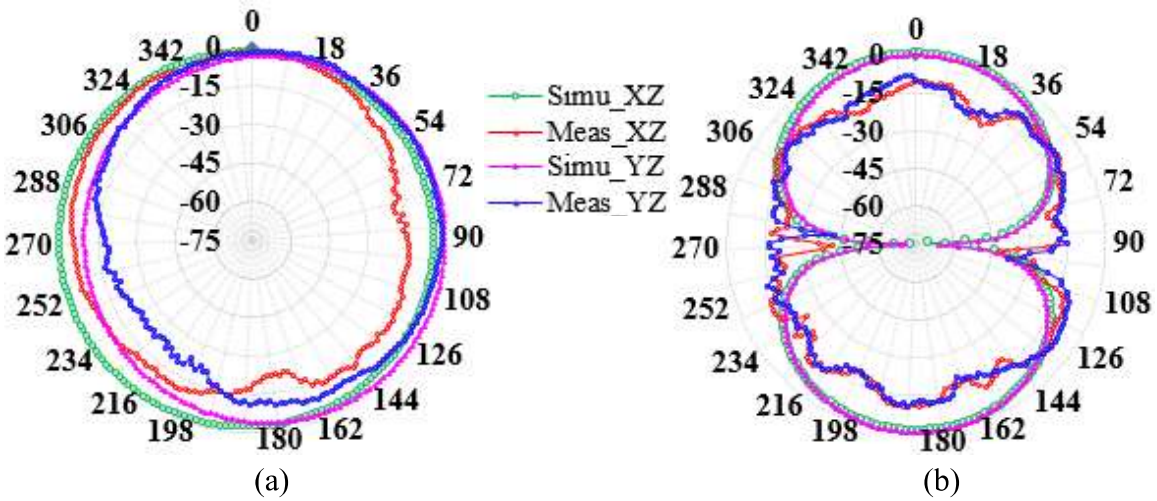

Fig. 2.7: Simulated and measured 2-D radiation patterns along xz-plane and yz-plane at 3.6 GHz, when element-1 is excited and element-2 is kept matched terminated (a) co-polarization and (b) cross-polarization.

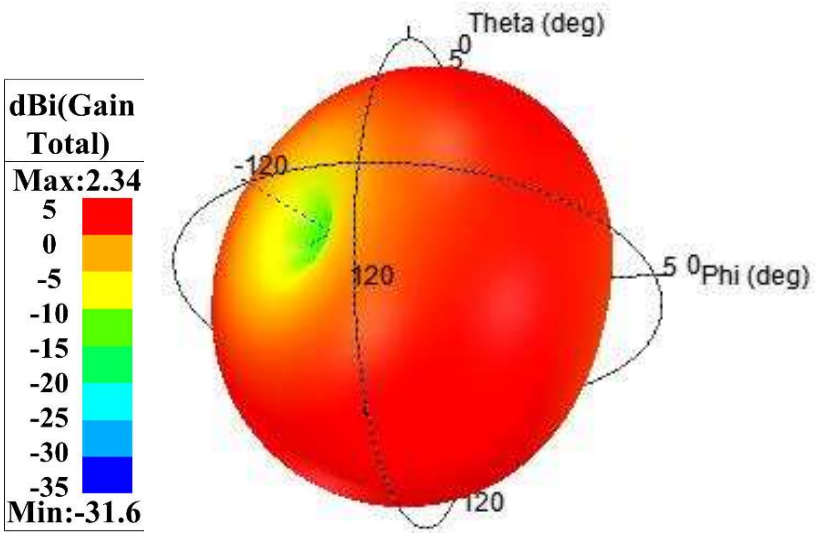

Fig. 2.8: 3-D radiation pattern for element-1 of the MIMO antenna at 3.6 GHz and element-2 is kept matched terminated.

2.3.3 Efficiency and Gain

The total efficiency of the i^{th} element and multiplexing efficiency of the two-element MIMO is estimated for high SNRs by the equation in [23], [25].

$$\eta_{tot(i)} = \eta_{rad(i)}\left(1-\sum_{j=1}^{2}\left|S_{ij}\right|^2\right) \tag{2.5}$$

$$\eta_{MUX} = \sqrt{(1-|\rho_c|^2)\eta_1\eta_2} \tag{2.6}$$

where $\eta_{rad(i)}$ is radiation efficiency of i^{th} element and ρ_c is complex correlation coefficient which is related to envelope correlation coefficient ρ_e, such as $\rho_c = |\rho_e|^{1/2}$ [62].

The simulated value of the radiation efficiency, total efficiency, multiplexing efficiency, and peak realized gain of the designed antenna at the frequency of 3.6 GHz are 93.2%, 92.9%, 91.8%, and 2.34 dBi, respectively. The plots of which are shown in Fig. 2.9. The measured value of realized gain at 3.6 GHz is 2.33 dBi.

2.3.4 Diversity Performances

To identify the correct behavior of the MIMO system, the analysis of some fundamental parameters (ECC, DG, MEG ratio, TARC, and CCL) are essential [27], [28], [30].

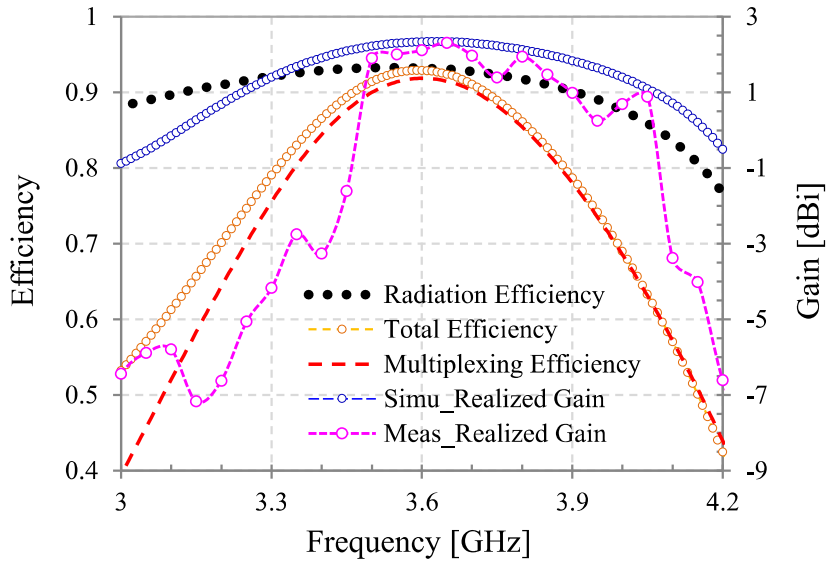

Fig. 2.9: Efficiency and gain of the MIMO antenna.

2.3.4.1 ECC, DG, and MEG Ratio

The simulated ECC and DG results are obtained by using both *S*-parameters and 3-D complex field equation. Whereas, the measured results of the ECC and DG are calculated by using *S*-parameters only, as illustrated in Fig. 2.10(a). The obtained values of ECC and DG are less than 0.012 and greater than 9.999 dB, respectively throughout the band.

The value of MEG_i/MEG_j should be close to unity and should not exceed ±3 dB for satisfactory MIMO performances. Fig. 2.10(b) shows that value of MEG_1/MEG_2 for the MIMO antenna is close to 1 throughout the band.

2.3.4.2 TARC and CCL

The TARC of the two-elements MIMO antenna is estimated using Eq. 2.7, that is

$$TARC = \sqrt{\frac{\left|(S_{11} + S_{12}e^{j\theta_2})\right|^2 + \left|(S_{21} + S_{22}e^{j\theta_2})\right|^2}{2}} \tag{2.7}$$

To investigate the TARC of MIMO antenna, the excitation of element-1 is kept at unity amplitude and zero phase, while element-2 is excited by similar amplitude but phase excitation of the element-2 is varied from 0° to 360° in seven cases, as considered Case-1 to Case-7.

Case-1: $P^1=0^\circ$, $P^2=0^\circ$, Case-2: $P^1=0^\circ$, $P^2=60^\circ$, Case-3: $P^1=0^\circ$, $P^2=120^\circ$, Case-4: $P^1=0^\circ$, $P^2=180^\circ$, Case-5: $P^1=0^\circ$, $P^2=240^\circ$, Case-6: $P^1=0^\circ$, $P^2=300^\circ$, Case-7: $P^1=0^\circ$, $P^2=360^\circ$.

Fig. 2.11(a) show that the obtained values of TARC (simulated and measured) for seven cases is less than 0.5 throughout the operating band. Both simulated and measured values are in close agreement.

The measured and simulated value of CCL are plotted in Fig. 2.11(b). It is observed that the obtained CCL is less than 0.5 bps/Hz.

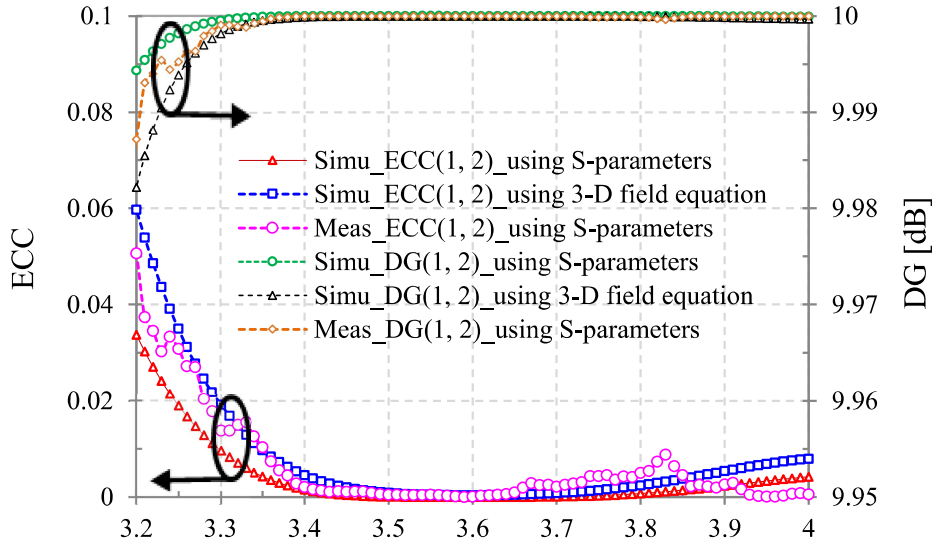

(a)

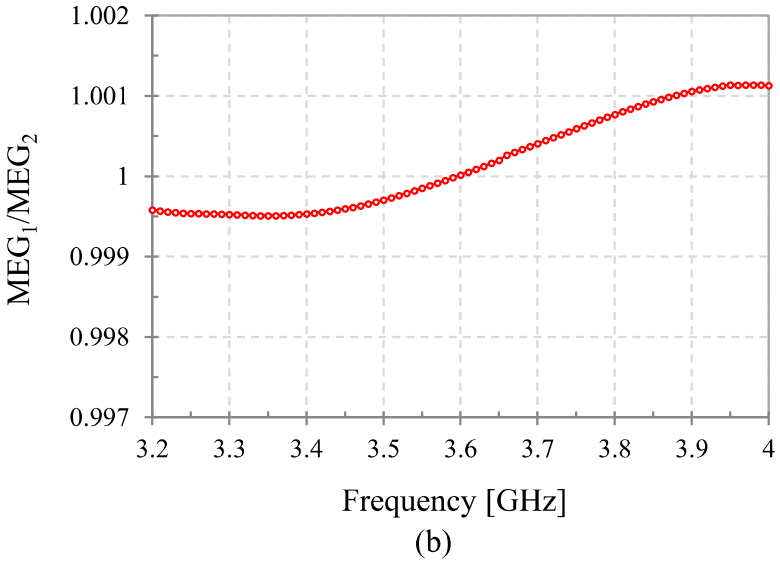

(b)

Fig. 2.10: For two-element MIMO antenna (a) ECC and DG, and (b) ratio of MEG.

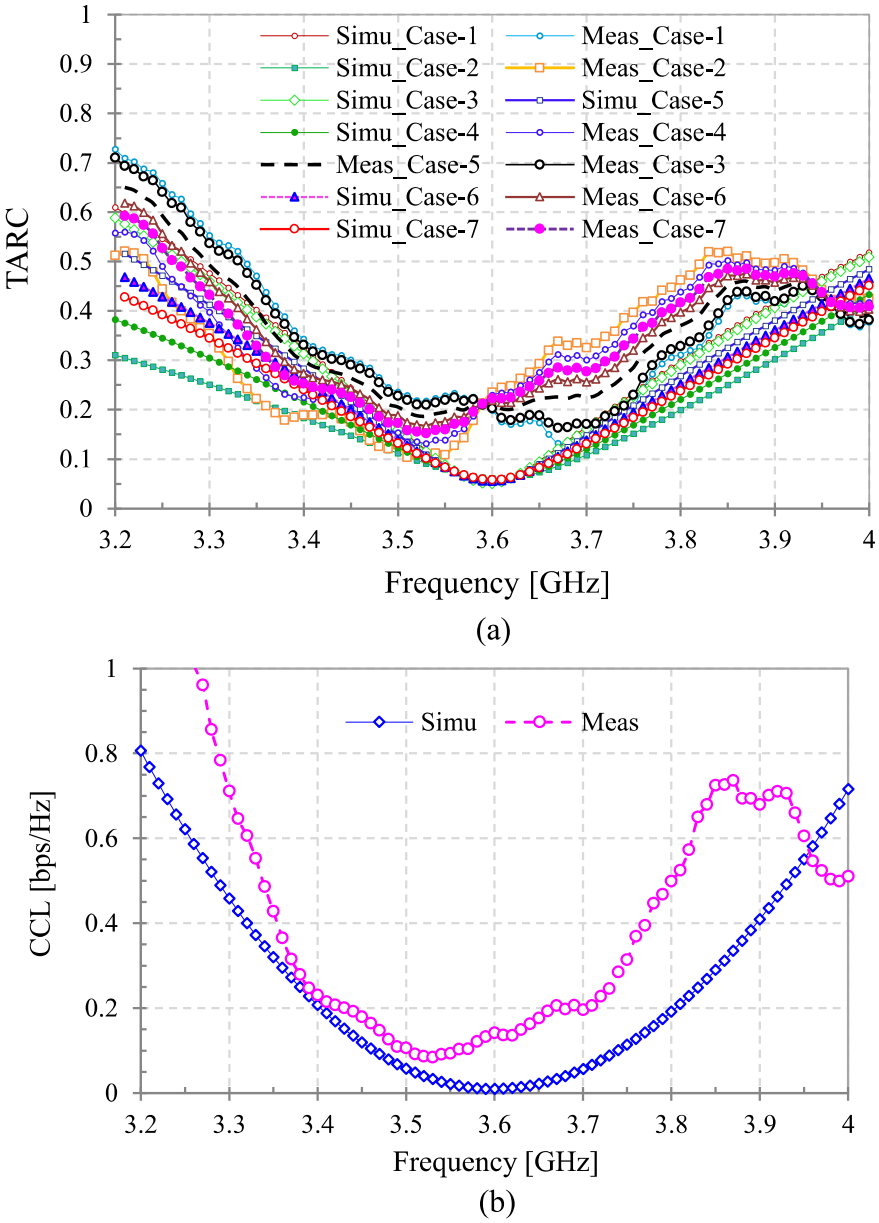

Fig. 2.11: For two-element MIMO antenna (a) TARC and (b) CCL.

2.3.5 Comparison and Review

Based on the obtained performances, the presented MIMO antenna is compared with the more desirable than the proclaimed literature as shown in Table 2.1. However, [60], [56], [101], and [107] have reported higher isolation values. It is due to the large area and volume occupied by the reported antennas. The antenna reported in [98] have occupied smaller area which is close to the proposed antenna. But the reported isolation value is ≥ 15 dB which is lower than the proposed antenna.

Table 2.1: Comparison between the proposed and similar reported two-element MIMO antenna

Ref.	**T_A** L×W (λ_H^2)	**A_V** L×W×h ($10^{-3}\lambda_H^3$)	**IBW** -10dB (GHz)	**D_{E-E}** (λ_H)	**I_{min}** (dB)	**P_D** (mm^3)
[93]	$0.70\lambda_H \times 1.12\lambda_H \cong 0.7777\lambda_H^2$	$0.70\lambda_H \times 1.12\lambda_H \times 0.0106\lambda_H \cong 8.2409\times10^{-3}\lambda_H^3$	4.183-6.584	$0.2008\lambda_H$	17	50×80×0.76
[98]	$0.23\lambda_H \times 0.37\lambda_H \cong 0.0846\lambda_H^2$	$0.23\lambda_H \times 0.37\lambda_H \times 0.0165\lambda_H \cong 1.3982\times10^{-3}\lambda_H^3$	3.1-10.6	$0.1058\lambda_H$	15	22×36×1.6
[60]	$0.25\lambda_H \times 0.42\lambda_H \cong 0.1042\lambda_H^2$	$0.25\lambda_H \times 0.42\lambda_H \times 0.0133\lambda_H \cong 1.3889\times10^{-3}\lambda_H^3$	2.5-14.5	$0.0707\lambda_H$	20	30×50×1.6
[64]	$0.57\lambda_H \times 0.71\lambda_H \cong 0.4025\lambda_H^2$	$0.57\lambda_H \times 0.71\lambda_H \times 0.0177\lambda_H \cong 7.1381\times10^{-3}\lambda_H^3$	5.32-5.64	$0.018\lambda_H$	16	32×40×1
[54]	$0.40\lambda_H \times 0.40\lambda_H \cong 0.1583\lambda_H^2$	$0.40\lambda_H \times 0.40\lambda_H \times 0.0165\lambda_H \cong 2.6168\times10^{-3}\lambda_H^3$	3.1-10.6	$0.0909\lambda_H$	15	38.5×38.5×1.6
[44]	$0.34\lambda_H \times 0.36\lambda_H \cong 0.1233\lambda_H^2$	$0.36\lambda_H \times 0.41\lambda_H \times 0.0083\lambda_H \cong 1.2358\times10^{-3}\lambda_H^3$	3.1-10.6	$0.0310\lambda_H$	16	35×40×0.8
[56]	$0.34\lambda_H \times 0.36\lambda_H \cong 0.1233\lambda_H^2$	$0.34\lambda_H \times 0.36\lambda_H \times 0.0083\lambda_H \cong 1.0195\times10^{-3}\lambda_H^3$	3.1-5	$0.0227\lambda_H$	22	33×35×0.8
[101]	$0.83\lambda_H \times 1.25\lambda_H \cong 1.0417\lambda_H^2$	$0.83\lambda_H \times 1.25\lambda_H \times 0.1525\lambda_H \cong 158.85\times10^{-3}\lambda_H^3$	2.5-2.7, 3.4-3.6	$0.0083\lambda_H$	25	100×150×18.3
[106]	$0.47\lambda_H \times 0.47\lambda_H \cong 0.2209\lambda_H^2$	$0.47\lambda_H \times 0.47\lambda_H \times 0.0188\lambda_H \cong 4.1529\times10^{-3}\lambda_H^3$	2.35-2.45	$0.1175\lambda_H$	18	60×60×2.4
[107]	$0.46\lambda_H \times 0.46\lambda_H \cong 0.2116\lambda_H^2$	$0.46\lambda_H \times 0.46\lambda_H \times 0.0491\lambda_H \cong 10.383\times10^{-3}\lambda_H^3$	2.3-2.8	$0.1188\lambda_H$	31	60×60×6.4
Prop.	$0.22\lambda_H \times 0.39\lambda_H \cong 0.0867\lambda_H^2$	$0.22\lambda_H \times 0.39\lambda_H \times 0.0089\lambda_H \cong 0.8501\times10^{-3}\lambda_H^3$	3.34-3.87	$0.1002\lambda_H$	20	20×35×0.8

Note: $\lambda_H = c/f_L$ being highest operating wavelength (f_L = lowest frequency of the antenna operation in GHz), T_A = total electrical area, A_V = overall antenna volume, IBW = impedance bandwidth, D_{E-E} = edge to edge distance between antenna elements, I_{mat} = impedance matching, I_{min} = minimum isolation, P_D = physical dimension.

2.4 Effect of Communication Environment

For the practical application of the proposed antenna, the two-element antenna is embedded with an extended ground plane (166×75 mm^2) and placed inside the device housing as illustrated in Fig. 2.12. To minimize the electrical conection effect, a 10×0.25 mm^2 copper strip is used to connect the ground of antenna and extended ground (PCB), shown in Fig. 2.12(a). The proposed antenna with extended ground is placed inside the acrylonitrile butadiene styrene ($\varepsilon_r = 2.3$) material based cubic box having thickness of 1 mm [98], shown in Fig. 2.12(b). The size of housing is 196×75×10 mm^3 which is choosen according to the dimentions of the propsed antenna with extended ground plane. The *S*-parameters performences is plotted in Fig. 2.12(c). The reflection coefficient is almost similar to the proposed antenna with significant shifting in resonant frequency towards lower side. However, the operating band is fully coverted in all the practical cases. The transmission coefficient is slightly affected but still satisfactory which is better than 15 dB. The radiation efficiency and realized gain in both cases are also satisfactory and almost close to the proposed antenna which is shown in Fig. 2.12(d).

2.5 Configuration of 12-element MIMO antenna

A new approach to design the 12-element MIMO antenna utilizing the proposed two-element MIMO antenna is presented in this section for 5G standard. The six pairs of two-element MIMO antenna are placed around the four side of the large ground (device PCB) having size 166×75 mm^2 on the same substrate. The distance between two successive two-element MIMO antenna placed on the larger edge of ground is 56 mm or 0.616λ_H (λ_H is highest operating wavelength at 3.3 GHz). A two-element MIMO antenna is placed on the smaller edge of the ground. The configuration of the 12-element MIMO antenna is shown in Fig. 2.13(a) corresponding *S*-parameter characteristics is plotted in Fig. 2.13(b).

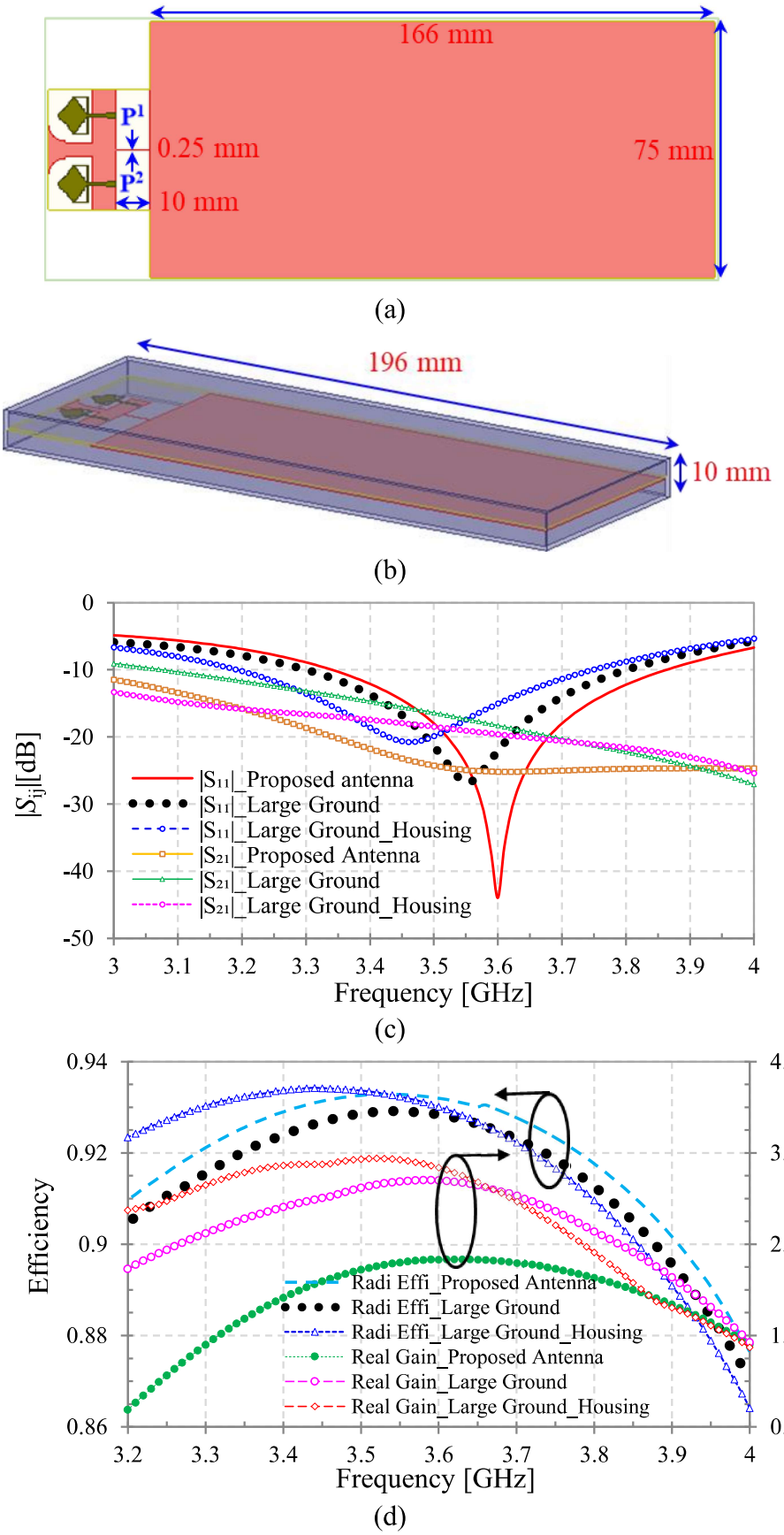

Fig. 2.12: Two-element MIMO with large ground (a) configuration, (b) with housing box, (c) corresponding simulated S-parameters characteristics, and (d) radiation efficiency and realized gain. Abbreviation: Radi Effi= radiation efficiency, Real = realized.

The 12-element MIMO antenna has a $S_{ij} \in i=j$ < -10 dB impedance bandwidth of 3.4-3.8 GHz and a minimum isolation value of 15 dB ($S_{ij} \in i \neq j$ < -15 dB) is successfully obtained between a pairs of elements. The reflection coefficient is almost similar and the transmission coefficient is slightly shifted but still satisfactory which is better than 15 dB to the proposed antenna. The radiation efficiency and realized gain of the 12-element MIMO antenna are better than the proposed two-element MIMO antenna, as shown in Fig. 2.14.

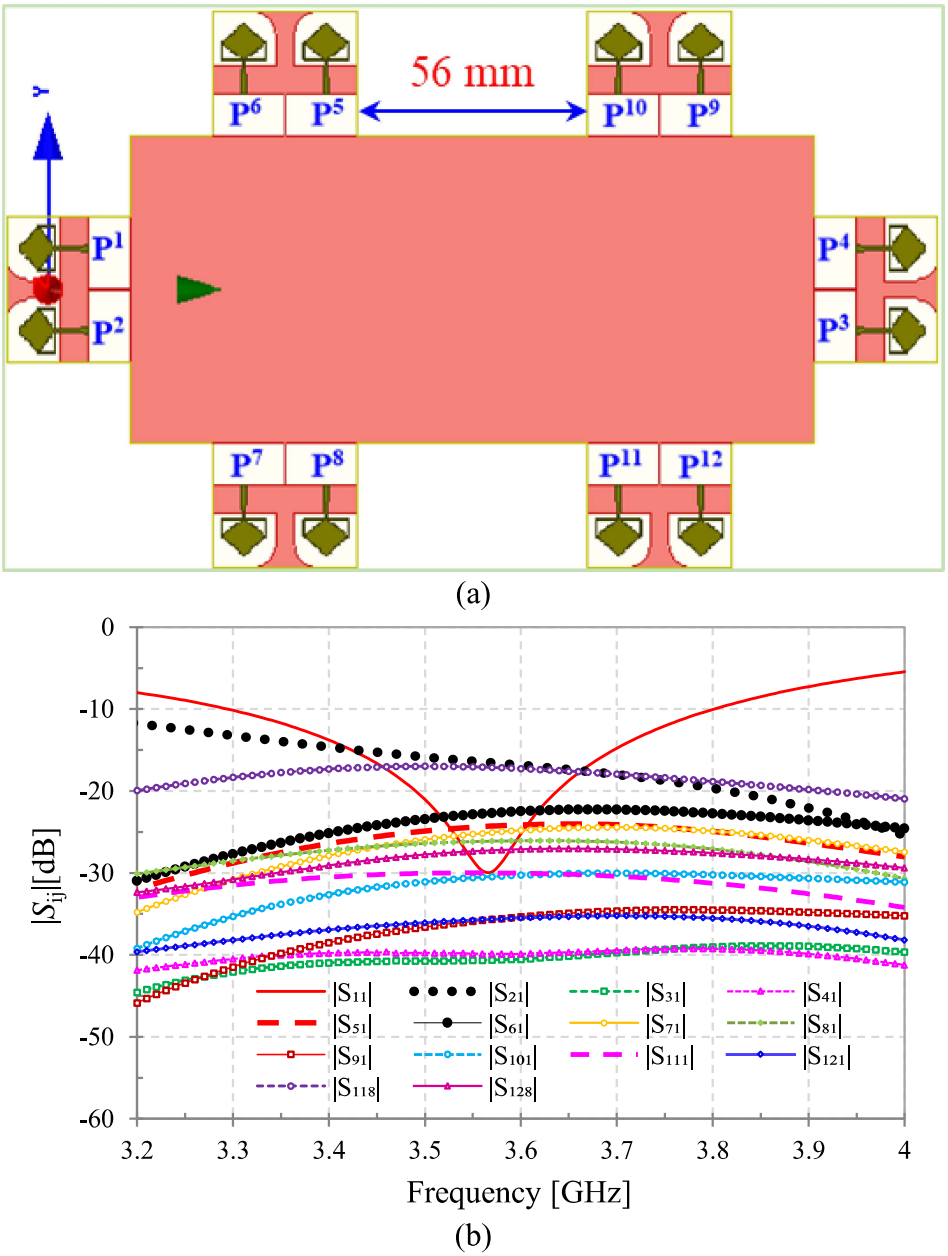

Fig. 2.13: 12-element MIMO antenna (a) configuration and (b) corresponding simulated *S*-parameters characteristics.

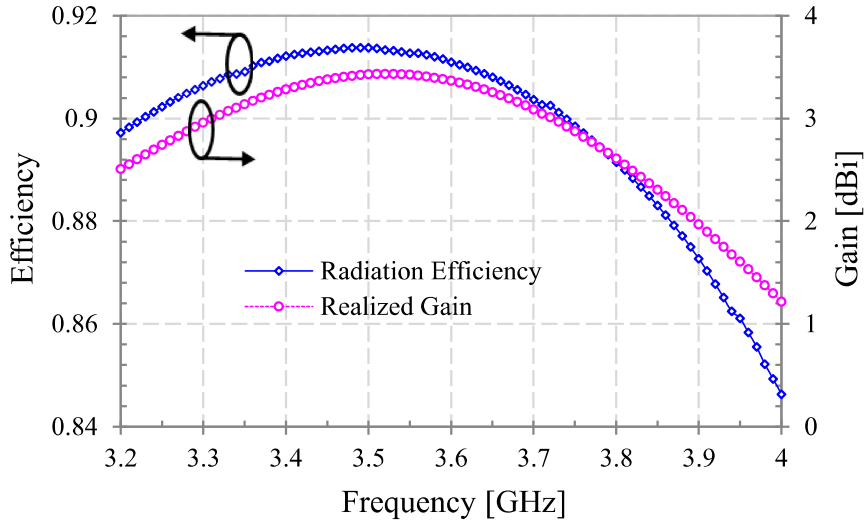

Fig. 2.14: 12-element MIMO antenna corresponding radiation efficiency and realized gain.

2.6 Summary

A closely spaced compact two-element MIMO antenna with simultaneous impedance matching and isolation enhancement is presented in this chapter. The designed antenna has a -10 dB impedance bandwidth of 530 MHz covering the entire band of sub-6 GHz 5G (3.34-3.87 GHz) with a minimum isolation value of 20 dB (simulated) and -15dB (measured) between antenna ports with impedance matching of -44 dB. The value of ECC < 0.012, DG > 9.999, the ratio of MEG $\cong 1$, TARC < 0.5, and CCL < 0.5 bps/Hz are observed throughout the band. The essential parameters (radiation characteristics, diversity performances, compact size, and ease of fabrication) of the designed two-element MIMO antenna are satisfactory. The housing effect on the two-element MIMO antenna is analyzed with an extended ground plane. The configuration of a 12-element MIMO antenna is proposed by utilizing two-element MIMO that can be useful for 5G wireless devices.

After successful implementation of 12-element MIMO antenna by utilizing two-element MIMO antenna, a compact wideband 20-element 3D-MIMO antenna for localization system is proposed by utilizing quad-element MIMO antenna in next chapter.